ACS Partner Journal

CHEMICAL & BIOMEDICAL IMAGING

pubs.acs.org/ChemBioImaging

Article

MR Molecular Imaging of Extradomain-B Fibronectin for Assessing Progression and Therapy Resistance of Prostate Cancer

Amita Vaidya, Aman Shankardass, Megan Buford, Ryan Hall, Peter Qiao, Helen Wang, Songqi Gao, Jiaoti Huang, Michael F. Tweedle, and Zheng-Rong Lu*

Cite This: *Chem. Biomed. Imaging* 2024, 2, 560−568

Read Online

ACCESS | Metrics & More | Article Recommendations

ABSTRACT: Accurate assessment and characterization of the progression and therapy response of prostate cancer are essential for precision healthcare of patients diagnosed with the disease. MRI is a clinical imaging modality routinely used for diagnostic imaging and treatment planning of prostate cancer. Extradomain B fibronectin (EDB-FN) is an oncofetal subtype of fibronectin highly expressed in the extracellular matrix of aggressive cancers, including prostate cancer. It is a promising molecular target for the detection and risk-stratification of prostate cancer with high-resolution MR molecular imaging (MRMI). In this study, we investigated the effectiveness of MRMI with an EDB-FN specific contrast agent MT218 for assessing the progression and therapy resistance of prostate cancer. Low grade LNCaP prostate cancer cells became an invasive phenotype LNCaP-CXCR2 with elevated EDB-FN expression after acquisition of the C-X-C motif chemokine receptor 2 (CXCR2). MT218-MRMI showed brighter signal enhancement in LNCaP-CXCR2 tumor xenografts with a ∼2-fold contrast-to-noise (CNR) increase than in LNCaP tumors in mice. Enzalutamide-resistant C4-2-DR prostate cancer cells were more invasive, with higher EDB-FN expression than parental C4-2 cells. Brighter signal enhancement with a ∼2-fold CNR increase was observed in the C4-2-DR xenografts compared to that of C4-2 tumors in mice with MT218-MRMI. Interestingly, when invasive PC3 prostate cancer cells developed resistance to paclitaxel, the drug-resistant PC3-DR cells became less invasive with reduced EDB-FN expression than the parental PC3 cells. MT218-MRMI detected reduced brightness in the PC3-DR xenografts with more than 2-fold reduction of CNR compared to PC3 tumors in mice. The signal enhancement in all tumors was supported by the immunohistochemical staining of EDB-FN with the G4 monoclonal antibody. The results indicate that MRMI of EDB-FN with MT218 has promise for detection, risk stratification, and monitoring the progression and therapy response of invasive prostate cancer.

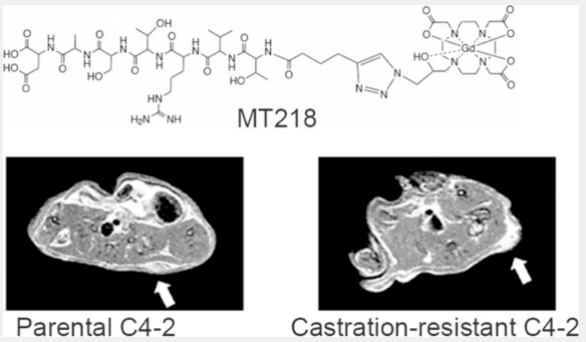

KEYWORDS: *MR molecular imaging, targeted contrast agent, MT218, extradomain B fibronectin, prostate cancer, active surveillance, drug resistance*

INTRODUCTION

Prostate cancer is the most common noncutaneous cancer in men and is the second leading cause of cancer deaths in the United States. An estimated quarter million men are diagnosed with prostate cancer in the United States every year.[1] Prostate cancer is a highly heterogeneous disease with significant variations in the molecular and pathological trajectory. Although one in eight men will be diagnosed with prostate cancer in their lifetime, most patients are diagnosed with low-risk cancer and with an indolent disease course without treatment. However, about one in five patients are diagnosed with high-risk cancer and have a substantial risk of prostate-cancer-related death.[2] The five-year survival rate of patients with localized disease is nearly 100%, while it drops dramatically to only 28% for those with distant metastases.[3] Therefore, accurate early detection, risk-stratification, and active surveillance of primary prostate cancer are critical to identify patients with high-risk disease and to monitor the status and progression of low-risk tumors for precision healthcare of prostate patients.

Currently, prostate specific antigen (PSA) screening, diagnostic imaging, and biopsy-based histology are routinely used for diagnosis of prostate cancer.[2,4−6] PSA testing is inconclusive,[7,8] and imaging and biopsy are followed for those with abnormal levels of PSA.[9] Transrectal ultrasound and

Received: January 5, 2024
Revised: May 29, 2024
Accepted: May 31, 2024
Published: June 11, 2024

https://doi.org/10.1021/cbmi.4c00002
Chem. Biomed. Imaging 2024, 2, 560−568

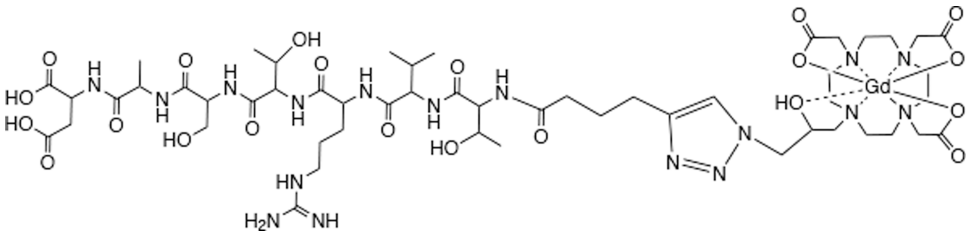

Figure 1. Structure of ZD2-N3-Gd(HP-DO3A), MT218.

multiparametric MRI (mpMRI) are the most commonly used imaging modalities for prostate cancer. However, these strategies have had limited success in localizing and differentiating high-risk prostate tumors from low-risk indolent tumors.[10] Prostate biopsy is still the gold standard for prostate cancer diagnosis. Unfortunately, the accuracy of prostate biopsy is often limited by inadequacies of prostate needle sampling due to the multifocal nature of the disease, the coexistence of various grades of tumors within the prostate, and the difficulty in assigning an accurate Gleason grade based on the minute sample size from the needle-biopsy. There is about 20% or higher risk of upgrading the score after radical prostatectomy compared with the original Gleason grade from the biopsy specimen. Consequently, most patients receive treatment even for low-risk disease to avoid potential undertreatment, which also leads to serious treatment-related long-term side-effects. In addition, prostate biopsies can lead to increased risks of hematuria, pain, infections, and septicemia. There is an unmet clinical need for a noninvasive imaging modality for accurate detection of high-risk prostate cancer and active surveillance for low-risk tumors for precision care of prostate cancer patients.

Molecular imaging of the markers associated with prostate cancer could overcome the limitations of the existing diagnostic methods and provide accurate detection, risk-stratification, and precision treatment of the disease. Recently, positron-emitting probes specific to prostate-specific membrane antigen (PSMA) ^{68}Ga-PSMA-11 and ^{18}F-DCFPyl have been approved for PET imaging of metastatic and recurrent prostate cancer.[11−13] However, their potential for staging or risk-stratification of primary prostate cancer has not been conclusively demonstrated in clinical studies.[14,15] In addition, PSMA expression can be absent in localized and metastatic tumors of some patients, which results in a false negative diagnosis with PSMA PET.

Extradomain B fibronectin (EDB-FN) is a cancer-associated isoform of fibronectin (FN) and is highly expressed in aggressive tumors, including high-risk prostate cancer. It is a marker of EMT, which is a biological program associated with invasion, metastasis, and drug resistance of multiple malignancies, including prostate cancer.[16−18] Elevated expression of EDB-FN is associated with EMT induction, cancer cell invasion, and metastasis.[16] It is overexpressed in various aggressive human cancers and absent in normal tissues.[19−22] Clinical evidence demonstrates that EDB-FN is overexpressed in the ECM of high-risk prostate cancer but not in benign lesions and benign prostatic hyperplasia.[23−25] EDB-FN is a promising oncotarget for developing molecular imaging technologies for the detection, risk-stratification, and active surveillance of high-risk prostate cancer.

MRI is a noninvasive clinical imaging modality and provides three-dimensional images of soft tissues with high spatial resolution. It is considered to be the most promising tool for prostate cancer imaging and well-suited for detecting localized tumors in the prostate.[26,27] mpMRI is currently the preferred imaging method for precision biopsy and surgery planning of prostate cancer.[28,29] The capability of MRI for precision diagnostic imaging is restrained by the lack of tumor specificity of the clinical contrast agents.[30] We have recently developed small peptide targeted gadolinium-based contrast agents specific to EDB-FN for MR molecular imaging (MRMI) of cancer.[31,32] A lead targeted macrocyclic agent ZD2-N3-Gd(HP-DO3A), or MT218, has been identified for clinical translation, Figure 1.[32,33] It has a higher T_1 relaxivity (6.54 mM^{-1} s^{-1}) than corresponding nontargeted clinical agent gadoteridol (4.1 mM^{-1} s^{-1}).[32] It produces stronger signal enhancement in rodent aggressive tumor models at a substantially reduced dose (0.04 mmol/kg) than the clinical agent (0.1 mmol/kg).[32,34] Our previous studies have shown that MRMI of EDB-FN is effective to differentiate high-risk tumors from low grade tumors in animal tumor models.[35,36]

In this study, we investigated the potential of MRMI of EDB-FN with MT218 for monitoring progression and development of therapy-resistance of prostate cancer. Timely assessment of disease progression and development of therapy resistance are essential for precision care of prostate cancer patients. Demonstration of the capability of MRMI with MT218 could expand its application for active surveillance and imaging-aided precision care in addition to detection and risk-stratification. We assessed the expression of EDB-FN in several pairs of prostate cancer cells, including LNCaP and LNCaP-CXCR2, C4-2 and drug resistant C4-2-DR, and PC3 and PC3-DR cells, in correlation with the invasiveness of the cells. We then evaluated the tumor signal enhancement of MRMI with MT218 in different prostate cancer tumor models, including LNCaP and LNCaP-CXCR2, and drug-resistant tumors. The potential of MRMI of EDB-FN for precision imaging, including monitoring disease progression and therapy-resistance, was determined in correlation with EDB-FN expression and the invasiveness of the cancer cells.

RESULTS

MRMI of EDB-FN for Monitoring Progression of Prostate Cancer

C-X-C motif chemokine receptor 2 (CXCR2) neuroendocrine tumor cells are enriched in high-grade and advanced prostate cancer. CXCR2 expression is associated with therapy resistance and progression of the disease.[37] It may also play a role in the EMT and ECM remodeling. Since EDB-FN is an oncogenic ECM protein associated with EMT, we evaluated the expression of EDB-FN in the LNCaP and LNCaP-CXCR2 prostate cancer cells to determine the potential correlation of EDB-FN with CXCR2. The CXCR2-positive LNCaP-CXCR2 was obtained by modifying the slow-growing LNCaP cells with

https://doi.org/10.1021/cbmi.4c00002
Chem. Biomed. Imaging 2024, 2, 560−568

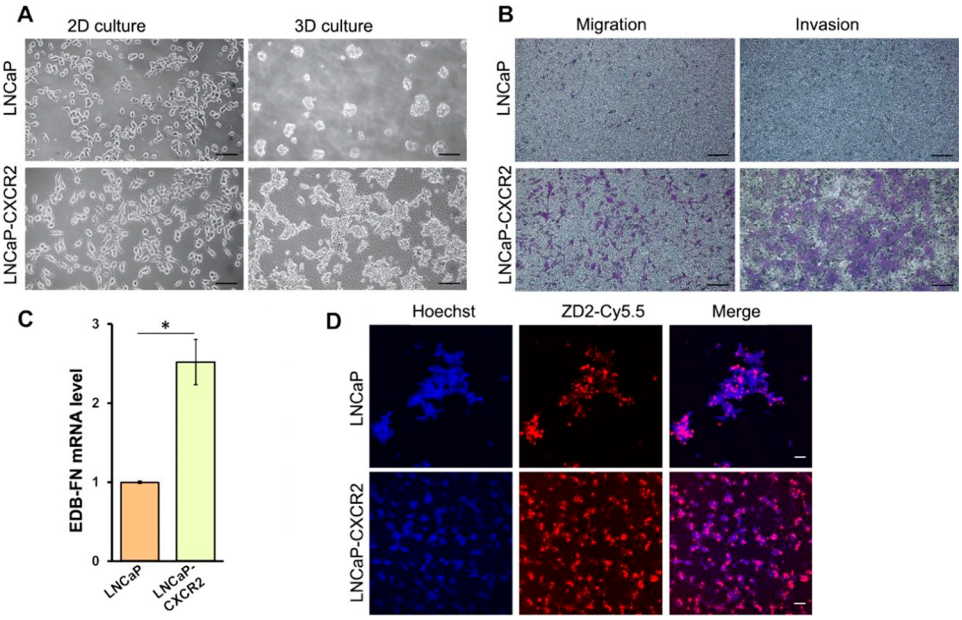

Figure 2. EDB-FN overexpression is associated with invasive prostate cancer cells that evolve from low-risk ones. Compared to the low-risk LNCaP cells, LNCaP-CXCR2 cells showed an elongated mesenchymal feature in 2D culture and high propensity to form 3D spheroids (A), increased migratory and invasive abilities indicated by strong purple color staining of the cells passing through a membrane filter (migration) and Matrigel layer (invasion; B), elevated expression of EDB-FN as measured by qRT-PCR (C), and strong ZD2-Cy5.5 binding (red fluorescence) of EDB-FN in 3D culture (D; $*p < 0.05$ using unpaired t test).

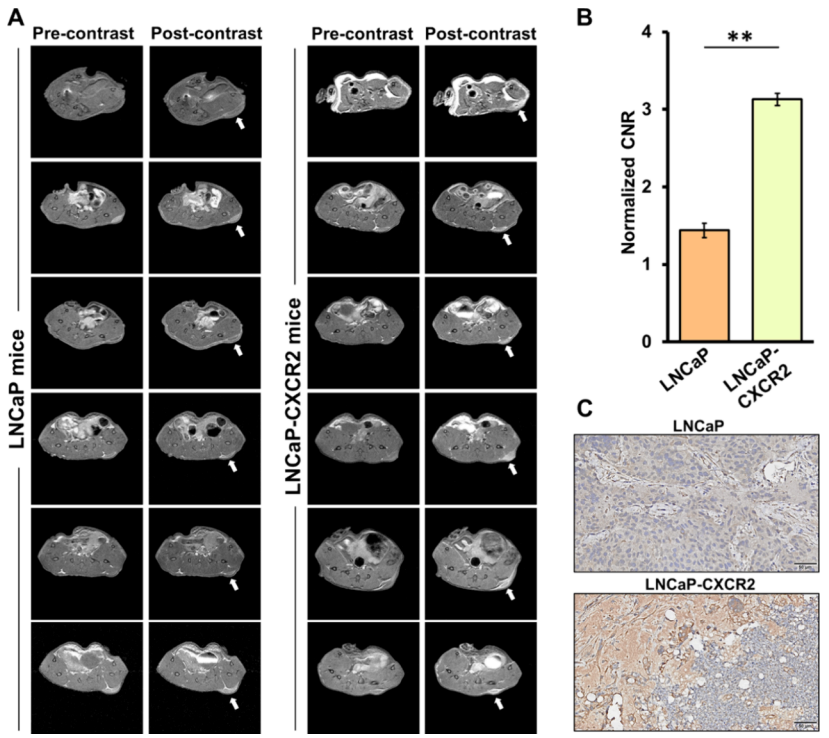

Figure 3. MRMI of EDB-FN with MT218 facilitates noninvasive assessment of the progression of low-risk prostate cancer. T_1-weighted 2D axial spin echo images were obtained before and 25 min postinjection of MT218 at 0.04 mmol/kg in athymic nu/nu mice bearing LNCaP and LNCaP-CXCR2 xenografts. Compared to the slow-growing LNCaP tumors, the invasive LNCaP-CXCR2 xenografts show brighter signal enhancement (A), significantly higher CNR (B, average of $n = 6$ mice, $**p < 0.05$ using unpaired t test), and strong EDB-FN staining in post-mortem IHC (C).

stable integration and overexpression of the pro-inflammatory and pro-tumorigenic IL8 receptor CXCR2.[37] LNCaP-CXCR2 cells also exhibited the mesenchymal feature, i.e., elongated cellular morphology, in 2D culture and were more invasive, i.e., larger spheroids, than the LNCaP cells, as shown in 3D culture (Figure 2A). Transwell assays showed that more LNCaP-CXCR2 cells (stained with a purple dye) migrated through a basement membrane and invaded through a Matrigel layer, indicating an increased invasiveness of the cells as compared to the LNCaP cells (Figure 2B). These increased aggressive

https://doi.org/10.1021/cbmi.4c00002
Chem. Biomed. Imaging 2024, 2, 560−568

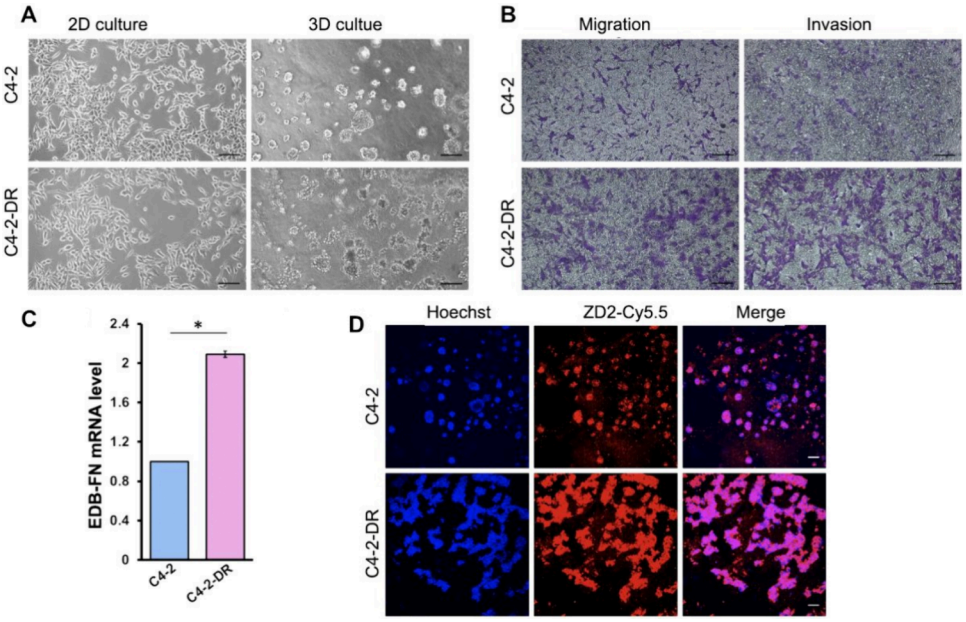

Figure 4. EDB-FN overexpression is associated with invasive prostate cancer cells that acquire resistance to androgen-deprivation therapy. Compared to their parent C4-2 cells, the enzalutamide-resistant C4-2-DR cells show comparable propensity to form 3D spheroids in 3D culture (A), increased migratory and invasive abilities (B), and significantly elevated expression of EDB-FN as measured by qRT-PCR (C) as well as ZD2-Cy5.5 binding in 3D culture (D; $*p < 0.05$ using unpaired t test).

features of LNCaP-CXCR2 cells were consistent with the previously reported results.[37] Correspondingly, LNCaP-CXCR2 cells exhibited significantly higher EDB-FN expression, as shown by RT-PCR as compared to the slow-growing parental LNCaP cells (Figure 2C). The staining of the 3D spheroids with the EDB-binding peptide fluorescence probe ZD2-Cy5.5 also showed stronger binding to LNCaP-CXCR2 spheroids (Figure 2D). The EDB-FN expression in LNCaP-CXCR2 cancer cells is correlated with their acquired invasiveness.

To assess the potential of MRMI of EDB-FN with MT218 to monitor the progression of the slow growing LNCaP prostate tumor to an invasive form after its acquisition of CXCR2, we performed MRI studies in mice bearing the LNCaP and LNCaP-CXCR2 prostate cancer xenografts after intravenous injection of MT218. Figure 3 shows the representative MRI images of LNCaP and LNCaP-CXCR2 prostate cancer xenografts established in athymic nu/nu mice. The images were acquired before and 25 min after intravenous injection of MT218 at 0.04 mmol/kg. Strong signal enhancement was observed in the invasive LNCaP-CXCR2 tumors, while only slight signal enhancement was observed in the low-grade LNCaP tumors (Figure 3A). Quantitative analyses of the signal intensities showed over 3-fold increased CNR in the LNCaP-CXCR2 tumors with MT218, while the LNCaP tumors had only about a 50% CNR increase (Figure 3B). Post-mortem immunohistochemical (IHC) analysis of the tumor tissues with an anti-EDB-FN G4 monoclonal antibody showed strong staining of EDB-FN in the LNCaP-CXCR2 tumors as compared to the low EDB-FN staining in the LNCaP tumor sections, indicating differential expression of EDB-FN in the LNCaP and LNCaP-CXCR2 tumors (Figure 3C). The IHC data corroborated the MRMI results, suggesting that MRMI of EDB-FN with MT218 is able to monitor the progression of slow growing prostate cancer to invasive tumors after acquisition of CXCR2.

MRMI of EDB-FN for Monitoring Enzalutamide-Resistance of Prostate Cancer

The expression of EDB-FN and its potential as a molecular marker for imaging therapy resistance was evaluated in C4-2 and enzalutamide-resistant C4-2-DR prostate cancer cells and tumor models. The C4-2-DR cells were an enzalutamide-resistant prostate cancer cell line generated by acquired resistance to 20 μM enzalutamide, an androgen-receptor antagonist.[37] Evaluation of the morphological and functional features of the cell lines demonstrated significantly increased propensity of C4-2 cells to form tumor spheroids in 3D culture compared to LNCaP cells (Figures 4A and 2A). Compared to C4-2 cells, C4-2-DR cells showed a similar 3D growth but significantly higher migration and invasion (Figure 4B). The C4-2-DR cells exhibited a significantly increased expression of EDB-FN over the C4-2 cells (Figure 4C). Additionally, in 3D culture, the resistant C4-2-DR cells were more invasive and showed proliferative tumor spheroids with significantly increased EDB-FN secretion compared to the C4-2 spheroids, evidenced by intense ZD2-Cy5.5 staining (Figure 4D).

MRMI showed bright tumor enhancement in C4-2 tumors in the mice at 25 min postinjection of MT218 (0.04 mmol/kg) as compared the precontrast tumors, while brighter signal enhancement was seen in the more invasive enzalutamide-resistant EDB-FN-rich C4-2-DR tumors (Figure 5A). Quantitative analyses of the signal intensities showed that MT218 at the same dose resulted in an over 5-fold CNR increase in the C4-2-DR tumors as compared to about a 2.5 CNR increase in the C4-2 tumors. C4-2-DR tumors had about a 2-fold higher CNR increase over their nonresistant C4-2 counterparts, indicating elevated EDB-FN expression in the drug-resistant tumors (Figure 5B). Post-mortem IHC analysis of EDB-FN also showed significantly elevated levels of EDB-FN expression in the drug-resistant tumors over the C4-2 tumors. The results correlated well with the differential signal enhancement in the C4-2 and C4-2-DR tumors, indicating that

https://doi.org/10.1021/cbmi.4c00002
Chem. Biomed. Imaging 2024, 2, 560−568

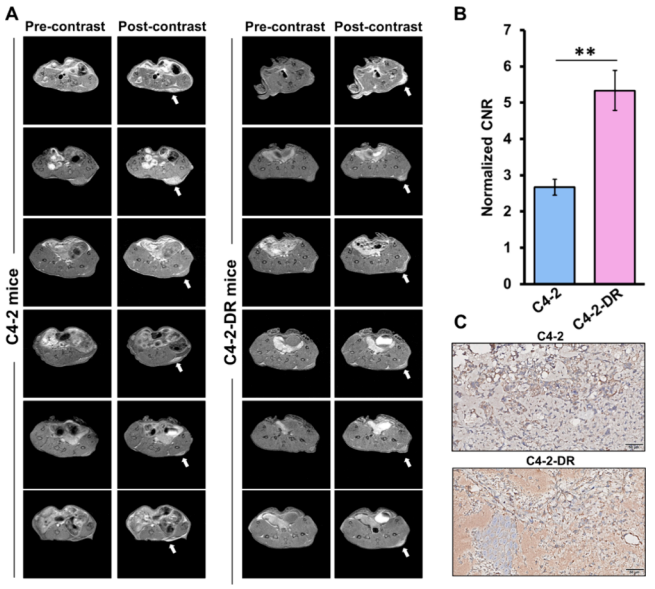

Figure 5. MRMI of EDB-FN MT218 facilitates noninvasive assessment of the development of resistance to anti-androgen therapy in prostate cancer. T_1-weighted 2D axial spin echo images were obtained before and 25 min postinjection of MT218 (0.04 mmol/kg) in athymic nu/nu mice. Compared to the nonresistant C4-2 tumors, enzalutamide-resistant C4-2-DR xenografts showed robust signal enhancement (A), significantly elevated CNRs (B, average of $n = 6$ mice, $^{**}p < 0.01$ using unpaired t test), and strong EDB-FN staining in post-mortem IHC (C).

MRMI of EDB-FN with MT218 has the promise to monitor the development of resistance to antiandrogen therapy in prostate cancer.

MRMI of EDB-FN for Assessing Paclitaxel-Resistant PC3 Prostate Cancer

PC3 prostate cancer cells are a PSMA-negative and highly aggressive cell line that is commonly used as an aggressive tumor model in prostate cancer research. Interestingly, PC3-DR cells, which were generated from PC3 cells by acquired resistance to 200 nM paclitaxel, showed a different trend with decreased ability for invasion as compared to the parental PC3 cells.[38] This observation exemplifies the heterogeneous natures of prostate cancer. We investigated the ability of MRMI of EDB-FN for characterizing decreased invasiveness of the PC3-DR tumors *in vivo*. PC3-DR cells showed no change in 2D and 3D growth and increased migration as compared with PC3 cells (Figure 6A). Interestingly, PC3-DR cells demonstrated a decreased ability to invade Matrigel-coated membranes (Figure 6B). EDB-FN expression was significantly reduced in PC3-DR cells as compared to parental cells (Figure 6C) as well as reduced staining of EDB-FN in the spheroids with ZD2-Cy5.5 (Figure 6D).

Figure 7A shows T_1-weighted axial spin−echo images of PC3 and PC3-DR tumors before and after the injection of MT218 at 0.04 mmol/kg. PC3 tumors showed robust signal enhancement and about 4-fold CNR increase with MT218, consistent with previous observations.[32,33] In contrast, the PC3-DR tumors only showed moderately enhanced signal enhancement and a 1.5-fold CNR increase over the precontrast images ($p = 0.07$). The invasive PC3 tumors showed significantly higher CNR with contrast enhancement by MT218 than that of the less invasive PC3-DR tumors (Figure 7B). The imaging results were further validated by the strong immunohistochemical EDB-FN staining in the invasive PC3 tumors over the less-invasive PC3-DR ones (Figure 7C), suggesting that EDB-FN upregulation is associated only with the invasiveness of prostate cancer, irrespective of drug resistance.

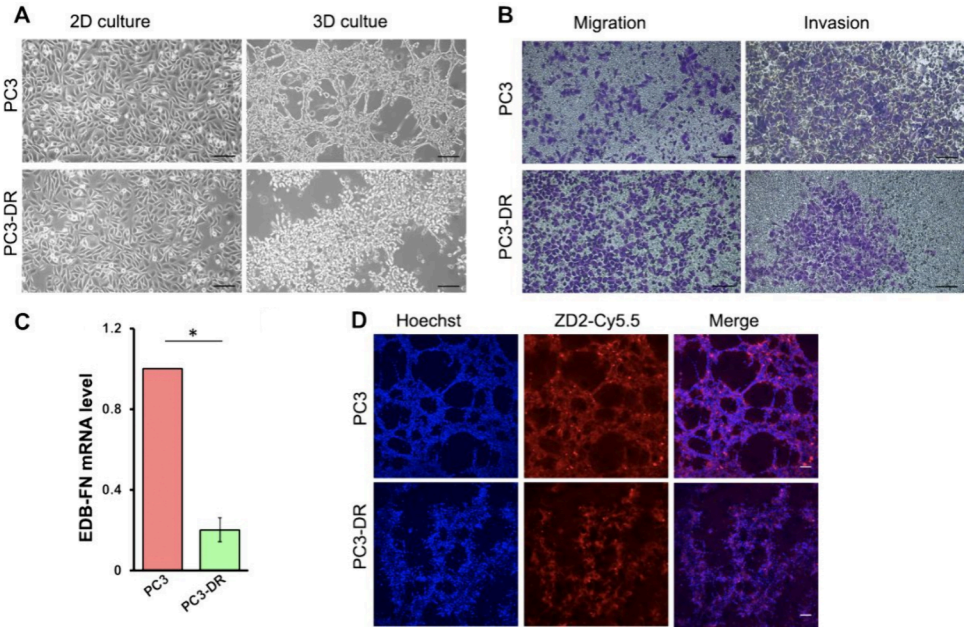

Figure 6. EDB-FN overexpression is not associated with paclitaxel-resistant prostate cancer cells that do not acquire invasive abilities. Compared to their high-risk parent PC-3 cells, PC3-DR cells show comparable propensity to form 3D spheroids in 3D culture (A) and increased migratory but decreased invasive abilities (B). The decreased invasion of taxane-resistant PC3-DR cells is accompanied by significant downregulation of EDB-FN, as measured qRT-PCR (C) and ZD2-Cy5.5 binding to EDB-FN in 3D culture (D; $^{*}p < 0.05$ using unpaired t test).

https://doi.org/10.1021/cbmi.4c00002
Chem. Biomed. Imaging 2024, 2, 560−568

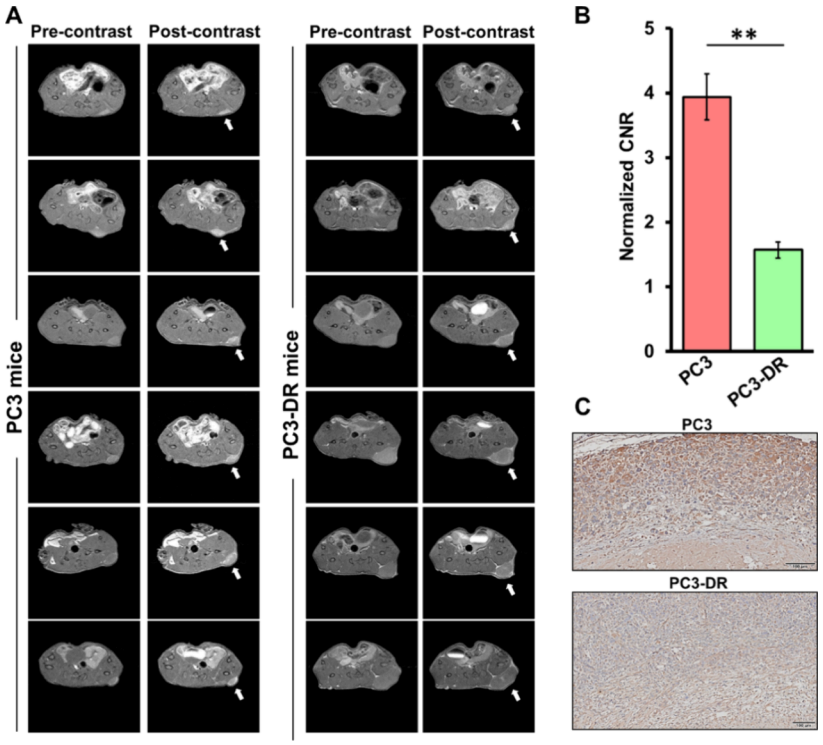

Figure 7. MRMI of EDB-FN with MT218 facilitates noninvasive assessment of noninvasive drug-resistant prostate cancer. T_1-weighted 2D axial spin echo images were obtained before and 25 min postinjection of MT218 (0.04 mmol/kg) in athymic nu/nu mice. Compared to high-risk PC3 tumors, noninvasive drug-resistant PC3-DR xenografts show reduced signal enhancement (A), significantly lower CNRs (B, average of $n = 6$ mice, $^{**}p < 0.01$ using unpaired t test), and weaker EDB-FN staining in post-mortem IHC (C).

DISCUSSION

Molecular imaging of the biological signatures of the initiation, proliferation, and invasion of prostate cancer has long been sought for accurate noninvasive characterization of prostate cancer to guide personalized care and treatment. MRI is advantageous over other imaging modalities for diagnostic imaging and treatment planning of localized prostate cancer due to its high spatial resolution for visualizing soft tissues. The challenge for MRMI of cancer is the low sensitivity of contrast enhanced MRI and the low concentration of the protein markers expressed on cancer cell surface. Although targeted macromolecular and nanosized paramagnetic agents have been developed for MRMI of cancer, clinical translation of these agents is hindered by several drawbacks, including slow excretion and potential toxic side effects associated with slow excretion. MT218 is a conjugate of a small linear peptide of seven amino acids (Thr-Val-Arg-Thr-Ser-Ala-Asp) to a clinical macrocyclic contrast agent Gd(HP-DO3A), one of safest GBCAs used in clinical practice.[39] MT218 specifically binds to oncoprotein EDB-FN in the ECM of aggressive tumors including prostate cancer. The abundant presence of EDB-FN in the ECM of aggressive tumors allows ready access of freely diffusible, hydrophilic small molecule like MT218. Efficient binding of MT218 and rapid clearance of unbound agent generate robust contrast enhancement in EDB-FN rich tumors in MRMI. Thus, MRMI with MT218 overcomes the limitations of targeting biomarkers expressed only on cancer cell surface. In addition, the small size and moderate binding affinity of MT218 allow rapid excretion after diagnostic imaging to minimize tissue retention of the bound MT218 and avoid any toxic side effects from long-term gadolinium retention.

Heterogeneity of prostate cancer presents a major challenge for the precision healthcare of patients. Accurate risk-stratification and active surveillance play a major role in identifying high-risk prostate cancer and monitoring low-grade tumors in the clinical management of the disease. Previously, we demonstrated that MT218-MRMI could effectively differentiate invasive PC3 prostate tumors from slow-growing LNCaP tumors in mice and rats.[32,33] This study further explored the potential of MT218-MRMI for active surveillance or monitoring the progression and therapy response of prostate cancer in six tumor models that exhibited a variety of invasivenesses, representing the heterogeneous nature of the disease. Among these models, LNCaP-CXCR2 and LNCaP represented a progression of low-grade prostate cancer into an invasive phenotype associated with an increased expression of CXCR2. C4-2, C4-2-DR, PC3, and PC3-DR represented heterogeneous progression of the disease in response to different treatments. Consistent with our previous observation in other cancer models,[16,36,40,41] the expression levels of EDB-FN correlated well with the invasiveness of the prostate cancer cell lines. EDB-FN expression was significantly higher in the invasive LNCaP-CXCR2, C4-2-DR, and PC3 cells than in the correspondingly less invasive LNCaP, C4-2, and PC3-DR cells. MT218-MRMI provided accurate characterization of the invasiveness of the tumor models based on the contrast enhancement and correlated with the EDB-FN expression levels in the tumors. The results further demonstrated the potential of MT218-MRMI for noninvasive risk-stratification of high-risk prostate cancer and also showed its promise for noninvasive active surveillance of low grade prostate cancer and monitoring tumor response to therapies.

https://doi.org/10.1021/cbmi.4c00002
Chem. Biomed. Imaging 2024, 2, 560−568

Currently, prostate biopsy is still the gold standard for diagnosis, risk-stratification, and active surveillance of prostate cancer in clinical practice. Imaging modalities, including transrectal ultrasound and mpMRI, are routinely used to improve the accuracy of prostate biopsy and diagnosis. However, MRI guided biopsy still suffers from inaccuracy, including underdiagnosis of some tumors.[42] Clinical application of a cancer-specific MRI contrast agent may improve diagnostic accuracy. MT218 is able to produce robust contrast enhancement in aggressive tumors and differentiate aggressive prostate cancer from low grade tumors in preclinical models at a substantially reduced dose, 0.04 mmol/kg vs 0.1 mmol/kg of a clinical GBCA.[32] The low effective dose of MT218 is clearly a safety advantage over the clinical agents in addition to its specificity for aggressive tumors. The effectiveness of MRMI with MT218 for the precision imaging of high-risk prostate cancer needs to be demonstrated in extensive clinical trials before clinical implementation in diagnostic imaging of prostate cancer. Currently, MT218 is in clinical trials for the MRMI of solid tumors. The phase 1 clinical trial in healthy men showed an excellent safety profile and pharmacokinetics indistinguishable from those of clinical contrast agents.[43] Later phase clinical trials are underway to assess its feasibility for detecting EDB-FN positive prostate cancer in patients.

CONCLUSION

We have further demonstrated that EDB-FN is an ECM marker of invasive prostate cancer. We have previously demonstrated that MT218-MRMI is promising for the detection and risk stratification of invasive prostate cancer. This study has shown that it also has potential to noninvasively assess progression of a low-grade prostate tumor to an invasive cancer and to monitor tumor response to therapies, whether the tumor becomes a more invasive therapy-resistant phenotype or a less invasive resistant phenotype based on the changes of EDB-FN levels in the tumors. MRMI of EDB-FN with MT218 has promise for detection, risk stratification, and assessment of progression and therapy response of invasive prostate cancer.

MATERIALS AND METHODS

Cell Culture

Prostate cancer cell lines LNCaP, C4-2, and PC3 were purchased from ATCC (Manassas, VA). The paclitaxel-resistant derivative of PC3 (PC3-DR) was a kind gift from Dr. Aaron Mohs (University of Nebraska, Omaha, NE). LNCaP-CXCR2 and enzalutamide-resistant C4-2-DR cells were developed in the lab of Dr. Jiaoti Huang (Duke University, Durham, NC) by stable integration of CXCR2 plasmid and with resistance to 25 μM enzalutamide (SelleckChem, Houston TX), respectively.[37] The prostate cancer cell lines were cultured in RPMI1640 medium (Sigma, St. Louis, MO). Both of the media were supplemented with 10% fetal bovine serum and 100 units/mL of penicillin/streptomycin. All of the cells were cultured at 37 °C and 5% CO_2.

Invasion and Migration Assays

Transwell assays, with and without Matrigel, were performed to assess the invasive and migratory properties of the different PCa cells. To evaluate migration, 1×10^5 prostate cancer cells (starved overnight) were plated in transwell inserts (VWR, Radnor, PA). The next day, nonmigrated cells were removed by swabbing the insets, and the migrated cells at the bottom of the insets were fixed (10% formalin for 10 min) and stained with 0.1% crystal violet (20 min). The cells were imaged using a Moticam T2 camera after removal of excess stain and overnight drying. To evaluate the ability of the cells to invade through a basement membrane in addition to the transwell membranes, 100 μL of 0.5 mg/mL Corning Matrigel membrane matrix was added atop the transwell membrane and incubated at 37 °C to solidify and form a gel coating (Corning, NY). The cells (2×10^5) were starved overnight and seeded onto the gel coating, and the assay was performed as described above.

3D Culture and ZD2-Cy5.5 Staining

To test the ability of the prostate cancer cells to grow in a 3D Matrigel culture, 200 μL of Corning Matrigel membrane matrix was added to each well of an eight-well microslide (Ibidi, Fitchburg, WI) and incubated at 37 °C to solidify and form a gel coating. The cells (1×10^5) were seeded onto the gel coating in each well. 3D growth was monitored and imaged for up to 3 days by using the Moticam T2 camera. To evaluate the expression of EDB-FN, the 3D cultures were stained with 100 nM ZD2-Cy5.5 and 5 μg/mL Hoechst 33342 for 30 min. Excess stains were removed with PBS washes, and fluorescence microscopy was performed on an Olympus confocal microscope (Japan).

qRT-PCR

Total RNA was extracted from prostate cancer cells using the RNeasy Plus Mini Kit (Qiagen, Germantown, MD). Reverse transcription and qPCR were performed using the miScript II RT Kit (Qiagen, Germantown, MD) and SyBr Green PCR Master Mix (Thermo Fisher Scientific), respectively. Fold change expression was measured by the $2^{-\Delta\Delta Ct}$ method with β-actin as the housekeeping gene. The following primer sequences were used: EDB-FN: Fwd 5′-CCG CTA AAC TCT TCC ACC ATT A-3′, Rev 5′-AGC CCT GTG ACT GTG TAG TA-3′; β-actin: Fwd 5′-CAT CCA CGA AAC TAC CTT CAA CTC C-3′, Rev 5′-GAG CCG CCG ATC CAC ACG-3′.

Xenograft Mouse Models

Nude athymic mice (6-week-old nu/nu males) were purchased from The Jackson Laboratory (Bar Harbor, MA) and housed in the animal facility at CWRU. All the animal experiments were performed according to the protocol approved by the IACUC of CWRU. About $(5-6) \times 10^6$ LNCaP, LNCaP-CXCR2, C4-2, C4-2-DR, PC3, and PC3-DR cells suspended in a Matrigel-PBS mixture (1:1) were subcutaneously injected in the left flanks of nude mice (100 μL per mouse, six mice per group times six models = 36 mice). MRMI was performed on the six xenograft models with a 0.04 mmol/kg dose of MT218 after the tumors reached volumes of about 50−75 mm^3. After imaging, the animals were euthanized, and the tumors were harvested for post-mortem histology and immunohistochemistry (IHC).

MRMI of EDB-FN with MT218

MRMI was conducted in a 3T MRS 3000 scanner (MR Solutions, Surrey, UK) with a mouse short quad coil. The mice were anesthetized with isoflurane, and a tail vein catheter was setup. T_1-weighted MR images were obtained before (precontrast) and 25 min after injection (postcontrast) of 0.04 mmol/kg dose of MT218. The following two sequences were used with respiratory gating: axial fast spin echo (FSE; T_R = 305 ms, T_E = 11 ms, FA = 90°, FOV = 40 mm × 40 mm, slice thickness = 1 mm, slice number = 15, N_{av} = 2, matrix = 256 × 256) and coronal FSE (T_R = 305 ms, T_E = 11 ms, FA = 90°, FOV = 90 mm × 90 mm, slice thickness = 1 mm, slice number = 20, N_{av} = 1, matrix = 248 × 512). Contrast-to-noise ratios (CNRs) were calculated using the following formula: (average tumor intensity − average muscle intensity)/standard deviation of noise. Image and CNR analyses were performed using FIJI (FIJI = Just ImageJ) software.

Immunohistochemistry

Staining and IHC services were provided by the Tissue Resources Core Facility of the Case Comprehensive Cancer Center (grant P30 CA43703). The tumor tissues were fixed in 10% neutral buffered formalin. Paraffin-embedded specimens were sectioned and H&E-stained to visualize morphology. IHC was performed using an anti-EDB-FN antibody G4 clone (1:100 dilution, Absolute Antibody, UK). All the slides were assessed by a certified pathologist.

https://doi.org/10.1021/cbmi.4c00002
Chem. Biomed. Imaging 2024, 2, 560−568

Statistical Analyses

All of the experiments were independently replicated at least three times ($n = 3$), unless otherwise stated. Data are represented as mean ± s.e.m. Statistical analysis was performed using Graphpad Prism. Data between two groups were compared using an unpaired Student's t test. $p < 0.05$ was considered to be statistically significant.

AUTHOR INFORMATION

Corresponding Author

Zheng-Rong Lu − *Department of Biomedical Engineering, Case Western Reserve University, Cleveland, Ohio 44106, United States; Case Comprehensive Cancer Center, Case Western Reserve University, Cleveland, Ohio 44106, United States;* orcid.org/0000-0001-8185-9519; Phone: (216) 268-0187; Email: zxl125@case.edu

Authors

Amita Vaidya − *Department of Biomedical Engineering, Case Western Reserve University, Cleveland, Ohio 44106, United States*

Aman Shankardass − *Department of Biomedical Engineering, Case Western Reserve University, Cleveland, Ohio 44106, United States*

Megan Buford − *Department of Biomedical Engineering, Case Western Reserve University, Cleveland, Ohio 44106, United States*

Ryan Hall − *Department of Biomedical Engineering, Case Western Reserve University, Cleveland, Ohio 44106, United States*

Peter Qiao − *Department of Biomedical Engineering, Case Western Reserve University, Cleveland, Ohio 44106, United States*

Helen Wang − *Department of Biomedical Engineering, Case Western Reserve University, Cleveland, Ohio 44106, United States*

Songqi Gao − *Molecular Theranostics LLC, Cleveland, Ohio 44103, United States*

Jiaoti Huang − *Department of Pathology, Duke University, Durham, North Carolina 27705, United States*

Michael F. Tweedle − *Wright Center of Innovation, Department of Radiology, The Ohio State University, Columbus, Ohio 43212, United States*

Complete contact information is available at: https://pubs.acs.org/10.1021/cbmi.4c00002

Notes

The authors declare the following competing financial interest(s): Gao, Hall, Lu, and Tweedle have ownership interest in Molecular Theranostics, LLC.

ACKNOWLEDGMENTS

This work was supported in part by the National Institutes of Health grants R44 CA265626 and R01 CA211762. This research was supported by the Tissue Resources Shared Resource of the Case Comprehensive Cancer Center (P30CA043703). Z.R.L. is the M. Frank Rudy and Margaret Domiter Rudy Professor of Biomedical Engineering at CWRU.

REFERENCES

(1) Siegel, R. L.; Miller, K. D.; Fuchs, H. E.; Jemal, A. Cancer Statistics, 2021. *CA Cancer J. Clin* **2021**, *71* (1), 7−33.

(2) Qaseem, A.; Barry, M. J.; Denberg, T. D.; Owens, D. K.; Shekelle, P. Screening for prostate cancer: a guidance statement from the Clinical Guidelines Committee of the American College of Physicians. *Ann. Int. Med.* **2013**, *158* (10), 761−769.

(3) Steele, C. B.; Li, J.; Huang, B.; Weir, H. K. Prostate cancer survival in the United States by race and stage (2001−2009): Findings from the CONCORD-2 study. *Cancer* **2017**, *123* (S24), 5160−5177.

(4) Litwin, M. S.; Tan, H. J. The Diagnosis and Treatment of Prostate Cancer: A Review. *JAMA* **2017**, *317* (24), 2532−2542.

(5) Ghafoor, S.; Burger, I. A.; Vargas, A. H. Multimodality Imaging of Prostate Cancer. *J. Nucl. Med.* **2019**, *60* (10), 1350−1358.

(6) Glass, A. S.; Cary, K. C.; Cooperberg, M. R. Risk-based prostate cancer screening: who and how? *Curr. Urol Rep* **2013**, *14* (3), 192−198.

(7) Moyer, V. A.; Force, U. S. P. S. T. Screening for prostate cancer: U.S. Preventive Services Task Force recommendation statement. *Ann. Int. Med.* **2012**, *157* (2), 120−134.

(8) Melnikow, J.; LeFevre, M.; Wilt, T. J.; Moyer, V. A. Counterpoint: Randomized trials provide the strongest evidence for clinical guidelines: The US Preventive Services Task Force and Prostate Cancer Screening. *Med. Care* **2013**, *51* (4), 301−303.

(9) Heijnsdijk, E. A.; der Kinderen, A.; Wever, E. M.; Draisma, G.; Roobol, M. J.; de Koning, H. J. Overdetection, overtreatment and costs in prostate-specific antigen screening for prostate cancer. *Br. J. Cancer* **2009**, *101* (11), 1833−1838.

(10) Glass, A. S.; Dall'Era, M. A. Use of multiparametric magnetic resonance imaging in prostate cancer active surveillance. *BJU Int.* **2019**, *124* (5), 730−737.

(11) True, L. D.; Chen, D. L. How Accurately does PSMA Inhibitor 18F-DCFPyL-PET-CT Image Prostate Cancer? *Clin. Cancer Res.* **2021**, *27*, 3512.

(12) Suh, M.; Im, H.-J.; Ryoo, H. G.; Kang, K. W.; Jeong, J. M.; Prakash, S.; Ballal, S.; Yadav, M. P.; Bal, C.; Jeong, C. W.; Kwak, C.; Cheon, G. J. Head to head comparison of (68)Ga-NGUL and (68)Ga-PSMA-11 in patients with metastatic prostate cancer: a prospective study. *J. Nucl. Med.* **2021**, *62*, 1457.

(13) Niaz, M. J.; Sun, M.; Skafida, M.; Niaz, M. O.; Ivanidze, J.; Osborne, J. R.; O'Dwyer, E. Review of commonly used prostate specific PET tracers used in prostate cancer imaging in current clinical practice. *Clin Imaging* **2021**, *79*, 278−288.

(14) Cook, G. J. R.; Kulkarni, M.; Warbey, V. S. PSMA PET/CT imaging for primary staging of intermediate and high-risk prostate cancer. *BJU Int.* **2019**, *124* (3), 357−358.

(15) Jochumsen, M. R.; Bouchelouche, K. PSMA PET/CT for Primary Staging of Prostate Cancer - An Updated Overview. *Semin Nucl. Med.* **2024**, *54* (1), 39−45.

(16) Vaidya, A.; Wang, H.; Qian, V.; Gilmore, H.; Lu, Z. R. Overexpression of Extradomain-B Fibronectin is Associated with Invasion of Breast Cancer Cells. *Cells* **2020**, *9* (8), 1826.

(17) Giannoni, E.; Bianchini, F.; Masieri, L.; Serni, S.; Torre, E.; Calorini, L.; Chiarugi, P. Reciprocal activation of prostate cancer cells and cancer-associated fibroblasts stimulates epithelial-mesenchymal transition and cancer stemness. *Cancer Res.* **2010**, *70* (17), 6945−6956.

(18) Nauseef, J. T.; Henry, M. D. Epithelial-to-mesenchymal transition in prostate cancer: paradigm or puzzle? Nature Reviews. *Urology* **2011**, *8* (8), 428−439.

(19) Kaspar, M.; Zardi, L.; Neri, D. Fibronectin as target for tumor therapy. *Int. J. Cancer* **2006**, *118* (6), 1331−1339.

(20) Inufusa, H.; Nakamura, M.; Adachi, T.; Nakatani, Y.; Shindo, K.; Yasutomi, M.; Matsuura, H. Localization of oncofetal and normal fibronectin in colorectal cancer, Correlation with histologic grade, liver metastasis, and prognosis. *Cancer* **1995**, *75* (12), 2802−2808.

(21) Menzin, A. W.; Loret de Mola, J. R.; Bilker, W. B.; Wheeler, J. E.; Rubin, S. C.; Feinberg, R. F. Identification of oncofetal fibronectin in patients with advanced epithelial ovarian cancer: detection in ascitic fluid and localization to primary sites and metastatic implants. *Cancer* **1998**, *82* (1), 152−158.

(22) Hall, R. C.; Vaidya, A. M.; Schiemann, W. P.; Pan, Q.; Lu, Z. R. RNA-Seq Analysis of Extradomain A and Extradomain B Fibronectin as Extracellular Matrix Markers for Cancer. *Cells* **2023**, *12* (5), 685.
(23) Jankovic, M. M.; Kosanovic, M. M. Fibronectin pattern in benign hyperplasia and cancer of the prostate. *Dis Markers* **2008**, *25* (1), 49−58.
(24) Suer, S.; Sonmez, H.; Karaaslan, I; Baloglu, H.; Kokoglu, E. Tissue sialic acid and fibronectin levels in human prostatic cancer. *Cancer Lett.* **1996**, *99* (2), 135−137.
(25) Albrecht, M.; Renneberg, H.; Wennemuth, G.; Moschler, O.; Janssen, M.; Aumuller, G.; Konrad, L. Fibronectin in human prostatic cells in vivo and in vitro: expression, distribution, and pathological significance. *Histochem Cell Biol.* **1999**, *112* (1), 51−61.
(26) Langer, D. L.; van der Kwast, T. H.; Evans, A. J.; Trachtenberg, J.; Wilson, B. C.; Haider, M. A. Prostate cancer detection with multi-parametric MRI: logistic regression analysis of quantitative T2, diffusion-weighted imaging, and dynamic contrast-enhanced MRI. *J. Magn Reson Imaging* **2009**, *30* (2), 327−334.
(27) Villers, A.; Lemaitre, L.; Haffner, J.; Puech, P. Current status of MRI for the diagnosis, staging and prognosis of prostate cancer: implications for focal therapy and active surveillance. *Curr. Opin Urol* **2009**, *19* (3), 274−282.
(28) Tosun, M.; Uslu, H. Prebiopsy multiparametric MRI and PI-RADS version 2.0 for differentiating histologically benign prostate disease from prostate cancer in biopsies: A retrospective single-center comparison. *Clin Imaging* **2021**, *78*, 98−103.
(29) Maggi, M.; Del Giudice, F.; Falagario, U. G.; Cocci, A.; Russo, G. I.; Di Mauro, M.; Sepe, G. S.; Galasso, F.; Leonardi, R.; Iacona, G. SelectMDx and Multiparametric Magnetic Resonance Imaging of the Prostate for Men Undergoing Primary Prostate Biopsy: A Prospective Assessment in a Multi-Institutional Study. *Cancers (Basel)* **2021**, *13* (9), 2047.
(30) Stavrinides, V.; Syer, T.; Hu, Y.; Giganti, F.; Freeman, A.; Karapanagiotis, S.; Bott, S. R. J.; Brown, L. C.; Burns-Cox, N.; Dudderidge, T. J.; et al. False Positive Multiparametric Magnetic Resonance Imaging Phenotypes in the Biopsy-naive Prostate: Are They Distinct from Significant Cancer-associated Lesions? *Lessons from PROMIS. Eur. Urol* **2021**, *79* (1), 20−29.
(31) Lu, Z. R.; Laney, V.; Li, Y. Targeted Contrast Agents for Magnetic Resonance Molecular Imaging of Cancer. *Acc. Chem. Res.* **2022**, *55* (19), 2833−2847.
(32) Li, Y.; Gao, S.; Jiang, H.; Ayat, N.; Laney, V.; Nicolescu, C.; Sun, W.; Tweedle, M. F.; Lu, Z. R. Evaluation of Physicochemical Properties, Pharmacokinetics, Biodistribution, Toxicity, and Contrast-Enhanced Cancer MRI of a Cancer-Targeting Contrast Agent, MT218. *Invest Radiol* **2022**, *57* (10), 639−654.
(33) Ayat, N. R.; Qin, J.-C.; Cheng, H.; Roelle, S.; Gao, S.; Li, Y.; Lu, Z.-R. Optimization of ZD2 Peptide Targeted Gd(HP-DO3A) for Detection and Risk-Stratification of Prostate Cancer with MRI. *ACS Med. Chem. Lett.* **2018**, *9* (7), 730−735.
(34) Ayat, N. R.; Vaidya, A.; Yeung, G. A.; Buford, M. N.; Hall, R. C.; Qiao, P. L.; Yu, X.; Lu, Z. R. Effective MR Molecular Imaging of Triple Negative Breast Cancer With an EDB-Fibronectin-Specific Contrast Agent at Reduced Doses. *Front Oncol* **2019**, *9*, 1351.
(35) Han, Z.; Li, Y.; Roelle, S.; Zhou, Z.; Liu, Y.; Sabatelle, R.; DeSanto, A.; Yu, X.; Zhu, H.; Magi-Galluzzi, C.; et al. Targeted Contrast Agent Specific to an Oncoprotein in Tumor Microenvironment with the Potential for Detection and Risk Stratification of Prostate Cancer with MRI. *Bioconjug Chem.* **2017**, *28* (4), 1031−1040.
(36) Han, Z.; Wu, X.; Roelle, S.; Chen, C.; Schiemann, W. P.; Lu, Z. R. Targeted gadofullerene for sensitive magnetic resonance imaging and risk-stratification of breast cancer. *Nat. Commun.* **2017**, *8* (1), 692.
(37) Li, Y.; He, Y.; Butler, W.; Xu, L.; Chang, Y.; Lei, K.; Zhang, H.; Zhou, Y.; Gao, A. C.; Zhang, Q.; et al. Targeting cellular heterogeneity with CXCR2 blockade for the treatment of therapy-resistant prostate cancer. *Sci. Transl Med.* **2019**, *11* (521), DOI: 10.1126/scitranslmed.aax0428.
(38) Liu, X.; Vaidya, A. M.; Sun, D.; Zhang, Y.; Ayat, N.; Schilb, A.; Lu, Z. R. Role of eIF4E on epithelial-mesenchymal transition, invasion, and chemoresistance of prostate cancer cells. *Cancer Commun. (Lond)* **2020**, *40* (2−3), 126−131.
(39) Tweedle, M. F. The ProHance story: the making of a novel MRI contrast agent. *Eur. Radiol* **1997**, *7* (S5), S225−S230.
(40) Nicolescu, C.; Kim, J.; Sun, D.; Lu, Z. R. Assessment of the Efficacy of the Combination of RNAi of lncRNA DANCR with Chemotherapy to Treat Triple Negative Breast Cancer Using Magnetic Resonance Molecular Imaging. *Bioconjug Chem.* **2024**, *35* (3), 381−388.
(41) Nicolescu, C.; Schilb, A.; Kim, J.; Sun, D.; Hall, R.; Gao, S.; Gilmore, H.; Schiemann, W. P.; Lu, Z. R. Evaluating Dual-Targeted ECO/siRNA Nanoparticles against an Oncogenic lncRNA for Triple Negative Breast Cancer Therapy with Magnetic Resonance Molecular Imaging. *Chem. Biomed Imaging* **2023**, *1* (5), 461−470.
(42) Ahdoot, M.; Wilbur, A. R.; Reese, S. E.; Lebastchi, A. H.; Mehralivand, S.; Gomella, P. T.; Bloom, J.; Gurram, S.; Siddiqui, M.; Pinsky, P.; et al. MRI-Targeted, Systematic, and Combined Biopsy for Prostate Cancer Diagnosis. *N Engl J. Med.* **2020**, *382* (10), 917−928.
(43) Li, Y.; Apseloff, G.; Tweedle, M. F.; Gao, S.; Henry, E.; Lu, Z. R. Pharmacokinetics and Tolerability of the Cancer-Targeting MRI Contrast Agent MT218 in Healthy Males. *Invest Radiol* **2024**, *59* (2), 165−169.